PJET, Vol. 1, No. 2, June 2023: 13-25
Poly Journal of Engineering and Technology
j o u r n a l h o m e p a g e : https://journals.bdu.edu.et/index.php/PJET/index
ORIGINAL ARTICLE

Synthesis and characterizations of Al-doped ZnO photocatalyst for removal dyes

Azimera Abireha[1], Nigus Gabbiye[1,*], Temesgen D. Desissa[2**], Ababay Ketema Worku[3]

[1]*Department of Chemical Engineering, Faculty of Chemical and Food Engineering, Bahir Dar Institute of Technology, Bahir Dar University, Bahir Dar, Ethiopia*

[2]*Department of Materials Science and Engineering, School of Mechanical, Chemical and Materials Engineering, Adama Science and Technology University, P.O.Box. 1888, Adama, Ethiopia*

[3]*Bahir Dar Energy Center, Bahir Dar Institute of Technology, Bahir Dar University, Bahir Dar P.O. Box 26, Ethiopia*

ABSTRACT

The disposal of organic dyes from different processing textile plants imposes series challenges to the environment and therefore to the health of society. Thus, these toxic and environmentally polluting organic dyes have to be amended before discharging them to the environment. In this work, ZnO and Al-doped ZnO photocatalytic materials were synthesized by the sol-gel method for removal of methylene blue (MB) organic dye from textile waste effluent. The phase purity and morphology of the synthesized samples were investigated by using X-ray diffraction (XRD) and Scanning Electron Microscopy (SEM)/Energy dispersive spectroscopy (EDS), respectively. Fourier Transform Infrared (FT-IR) Spectroscopy and UV visible (UV-VIS) spectroscopy were used, respectively, for chemical composition analysis and optical bandgap property measurements. FT-IR result showed predominant absorbance peaks at 864, 712, and 506 cm^{-1}, which correspond, respectively, to the Al-O, Al-O-Zn, and Zn-O bond stretching. From the absorbance spectra, the optical bandgap energies were calculated and found to be around 3.5, 3.0, 2.5, and 2.4 eV, respectively, for undoped, 0.5 %, 1%, and 2% Al-doped ZnO. The performance of the photocatalytic materials was investigated against the degradation ability towards the MB dye under different condition in a batch reactor. The 2%Al-doped ZnO exhibited the best performance with about 99 % degradation of MB under a light intensity of 5810 lux and corresponding reaction temperature of 65 °C.

Key words: Photocatalysis, Sol-gel process, methylene blue Dye, Al-doped ZnO catalyst.

DOI: https://doi.org/10.20372/pjet.v1i2.1242

Corresponding Authors:

[*]*Nigus Gabbiye, Faculty of Chemical and Food Engineering, Bahir Dar Institute of Technology, Bahir Dar University, P.O. Box 26, Bahir Dar, Ethiopia.*

Email: nigushabtu@gmail.com

[**]*Temesgen D. Desissa, Department of Materials Science and Engineering, School of Mechanical, Chemical and Materials Engineering, Adama Science and Technology University, P.O.Box. 1888, Adama, Ethiopia.*

Email:tamodeb@gmail.com

1. Introduction

Environment pollution by toxic substances is increasing from year-to-year due to increased manufacturing industries and processing chemical plants. Industrial effluents are the major pollutant sources to cause environmental pollution such as contaminations of water bodies. Based on their toxicity type, water body pollutants can be classified broadly as chemical, pathogenic and radioactive pollutants [1, 2]. Chemical pollutants (contaminants), among other types, could cause an enormous effect on human health due to their release in trace amounts from the industries to the environment [3]. Organic and inorganic pollutants are sub-classes of the chemical contaminant, where the former contaminant is one of the hazardous and non-biodegradable due to its physicochemical properties [1, 2]. Organic dyes are typical examples of organic contaminants, which are discharged from leather, paper, food, cosmetics industries to the environment, causing several health-related issues such as skin irritation, cancer, pregnancy problems, birth defects, and so on [4]. Moreover, these contaminants could cause challenges that could lead to ecological problems through the consumption of the oxygen molecules in the water bodies [5]. Therefore, these contaminants have to be amended and/or converted to non-toxic molecules as efficiently as possible before their discharge to the environment. Several conventional techniques such as flocculation, adsorption, coagulation, biodegradation, sedimentation, membrane process have been used for the removal and conversion of these contaminants. However, these techniques are insufficient due to the complex composition and different physicochemical properties of the contaminants as well as the low efficiency, high energy consumption, and risk of secondary pollutant [6-9]. Moreover, organic pollutants are non-degradable by traditional techniques due to the presence of stable aromatic groups in the structure of organic pollutants [1]. Therefore, an alternative technique with high efficiency, low energy consumption, and environmentally friendly is desirable for the treatment of the industrial effluents to amend and convert them to non-toxic molecules and substances. Advanced oxidation process such as Fenton, photo-Fenton and photocatalysis are an emerging technology to amend and/or degrade highly toxic organic pollutants. Photo-catalysis was uses photon energy and oxide semiconductor nanomaterials as catalysts to degrade organic contaminants through generating hydroxyl free radicals. Some of these oxide nanomaterials include titanium dioxide (TiO_2) [10, 11], zinc oxide (ZnO) [12-15], spinel structured ferrite materials (AB_2O_4, A= Zn, Co, B=Fe) [16-18], and other oxide nanoparticles for degradation of the organic dye from the industrial effluents. Most of these metal oxides used for the treatment of dye- contaminated wastewaters have large bandgap energy which usually requires operation in the UV range of the electromagnetic spectrum which is energy-intensive. However, through the introduction of dopant atoms, it is possible to narrow the optical band gap energy of these materials so that they can be active in the visible light range [19]. In this work, ZnO was doped with aluminum (Al) as a donor dopant to create additional energy levels in the bandgap energy of the material. Al donates an electron to Zn and therefore enhances its *n*-type properties, which could enhance its photocatalytic activity. The sol- gel method was employed to synthesize donor doped ZnO, i.e., $Zn_{1-x}Al_xO$ (x=0, 0.05, 0.01, and 0.2).

2. Materials and Methods

2.1. Materials

Zinc acetate dihydrate Zn $(CH_3COO)_2.2H_2O$ (98%, Sigma Aldrich), aluminum nitrate nonahydrate ($Al(NO_3)3.9H_2O$)) (98%, Sigma Aldrich), citric acid ($C_6H_8O_7$) (99.5%), methanol (CH_3OH)(99%), sodium hydroxide (NaOH) (99.8%), methylene blue ($C_{16}H_{18}ClN_3S$) (82%), and distilled water were utilized in this work.

2.2. Catalyst Synthesis by sol-gel method

Syntheses of Al-doped ZnO catalysts were performed using a similar synthesis procedure reported by Alias *et al*. [20]. Briefly, about 4.39 g of Zinc acetate dihydrate having a purity of 98% was dissolved in 99% pure of 100 mL methanol under

vigorous stirring at 25 °C for 2 h until a clear solution was obtained. The pH of the solution was varied from 6 to 9 through drop wise addition of 99.8% pure 1.0 M NaOH solution. The obtained sol was stirred vigorously for an hour and the sample was left at room temperature for about 48 h. Then, the supernatant was decanted and the gel was washed with distilled water, followed by centrifuging at 3000 rpm for about 30 minutes. After that, the sample was washed with distilled water to obtain a white precipitate, followed by drying the sample at room temperature. Finally, the dried sample was ground using mortar and pestles and the powder was subjected to Calcination at 650 °C for 4 h to remove impurities. The Al-doped ZnO was synthesized using the aforementioned procedure mentioned, where Al $(NO_3)_3.9H_2O$ was used as an aluminum dopant precursor through variation of the dopant percentage from 0.5% - 2%.

2.3. Characterizations

The phase purity of the samples was examined using X-ray powder diffraction (XRD-700, Shimadzu, South Korea) using copper Kα radiation ($\lambda_{CuK\alpha}$ = 1.5418 Å), a scan speed of 4.0 deg/min, 40 kV, 30 mA, and a 2-θ scanning range from 4–80°. The crystalline size (D) was obtained from XRD peaks using the following Scherrer equation (1).

$$D = \frac{(k\lambda)}{\beta \cos\theta} \tag{1}$$

The surface morphology and elemental composition of the samples were analyzed using an SEM-EDX (COXIEM-30, Shimadzu, South Korea). Fourier Transform Infrared Spectroscopy (FT-IR) (FT/IR-4000 series, JASCO) and Ultraviolet-visible Spectroscopy (UV-Vis) (PerkinElmer, lambda35) were used, respectively, to determine the functional group and the optical bandgap energy of the samples. The UV- Vis was performed in the range of 200–800 nm. Moreover, the UV-Vis spectroscopy was used to determine the concentration of the methyl blue dye (MB).

2.4. Degradation experiments

Batch photocatalytic degradation experiments were performed over ZnO and Al-doped ZnO catalysts for a wide range of operating parameters. For this commercially available dye, which is methylene blue, was used as model organic pollutant. Batch experiment setup was done using visible light source (fluorescent bulb) (**Figure 1**). The light source used were different sizes and was measured using digital luminance meter and found (3124, 4212, 5810 lux) for the dye degradation experiments. The synthesized catalysts performance tests were checked using different operating parameter. UV visible spectroscopy (PerkinElmer ultraviolet /visible spectrophotometer, lambda35) device was used to obtain absorbance of methylene blue as a function of wavelength. Finally, the calibration curve was plotted to obtain final concentrations of methylene blue after photocatalysts degradation experiment was established using a standard solution.

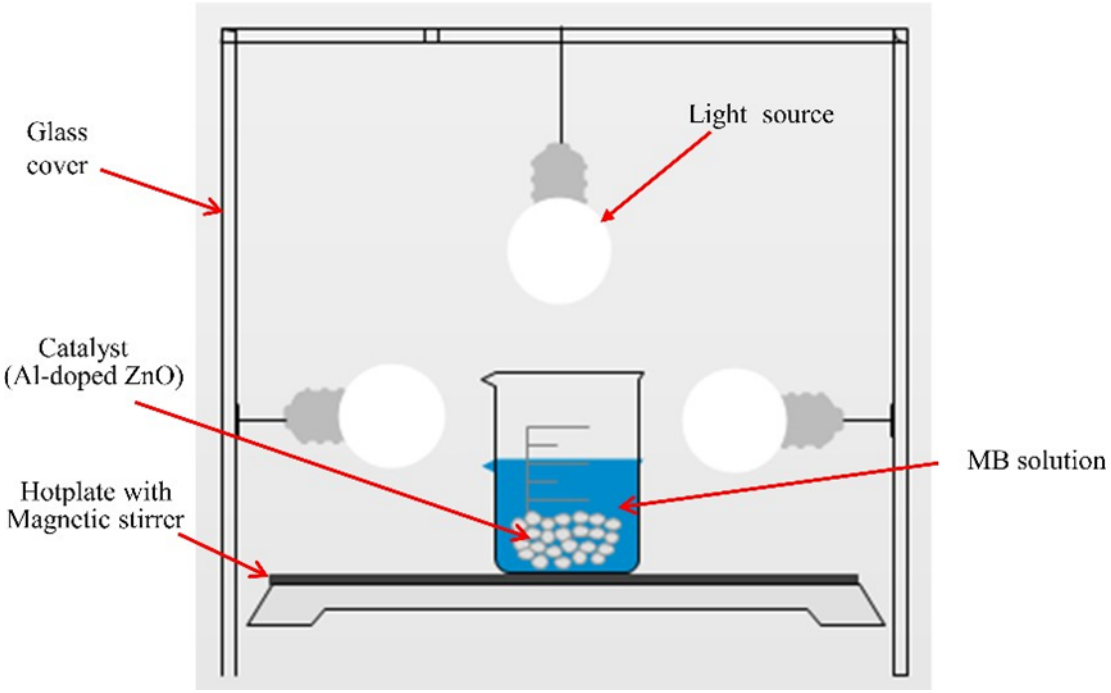

Figure 1: Schematic representation of the batch experimental setup.

Using UV-Vis spectroscopy, the initial concentration (C_i) of the MB was determined. Then, the concentration of the MB at any time interval (C_t) was measured after the dye was subjected to the degradation process. The degradation efficiency (η_D) can be expressed as a percentage of MB removal which can be calculated using following relation, equation (2) [21, 22].

$$\eta_D = \left(\frac{C_i - C}{C_i} \right) \times 100 \qquad (2)$$

3. Results and Discussions

3.1. Characterizations

The phase purity of un-doped and Al-doped ZnO samples were investigated using XRD and the result is presented in **Figure 2**. As it can be seen in figure 2, major diffraction peaks of the samples occurred at a 2θ of around 32, 34, 36, 47.5, 56.5, 63, 66, 68, 69, and 77 ° corresponding, respectively, to (100), (002), (101), (102), (110), (103), (200), (112), (201), and (202) crystallographic planes, in agreement with JCPDS 79-2205 [23, 24]. The crystal structure of the samples exhibited a hexagonal wurtzite structure [22-26] with a space group of *P63mc* (186). The slight angle shift to a higher 2θ compared to pure ZnO suggests successful incorporation of Al into the ZnO crystal structure.

.

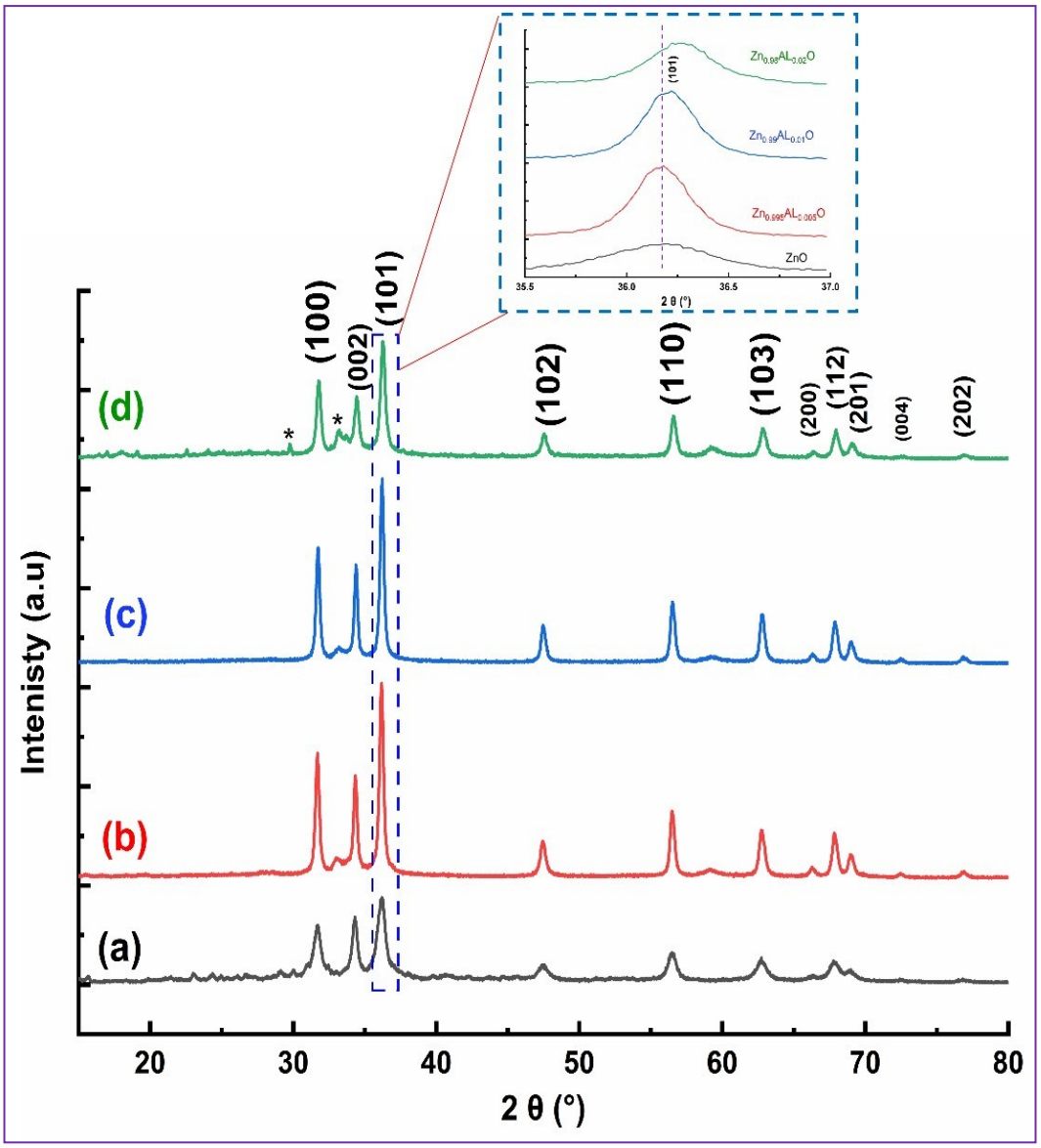

Figure 2: XRD peaks of ZnO and Al-doped samples. The inset shows the shift of peaks to a relatively higher 2θ.

Table1 shows the *d-spacing* of the samples in addition to the average crystallite size (*D*) – calculated from the Scherer equation – of the samples in (100) crystallographic planes.

Table1: The d-spacing and average crystallite size of pure ZnO and Al-doped ZnO for (100) planes.

Sample name	*2θ*	*d(Å)*	*Crystalline size, D (nm)*
ZnO	31.64	0.767	128
$Zn_{0.995}Al_{0.05}O$	31.70	0.794	262
$Zn_{0.99}Al_{0.1}O$	31.73	0.846	224
$Zn_{0.98}Al_{0.2}O$	31.81	0.944	225

The morphology of un-doped and Al-doped ZnO samples were analyzed as reported in **Figure 3**. It appears that there is a slight variation in the morphology of the samples when Al is incorporated into the crystal structure. This variation in their morphology comes due to Al metal ion in the ZnO NPs surface area or the replacement of Al^{3+} into Zn^{2+}sites.

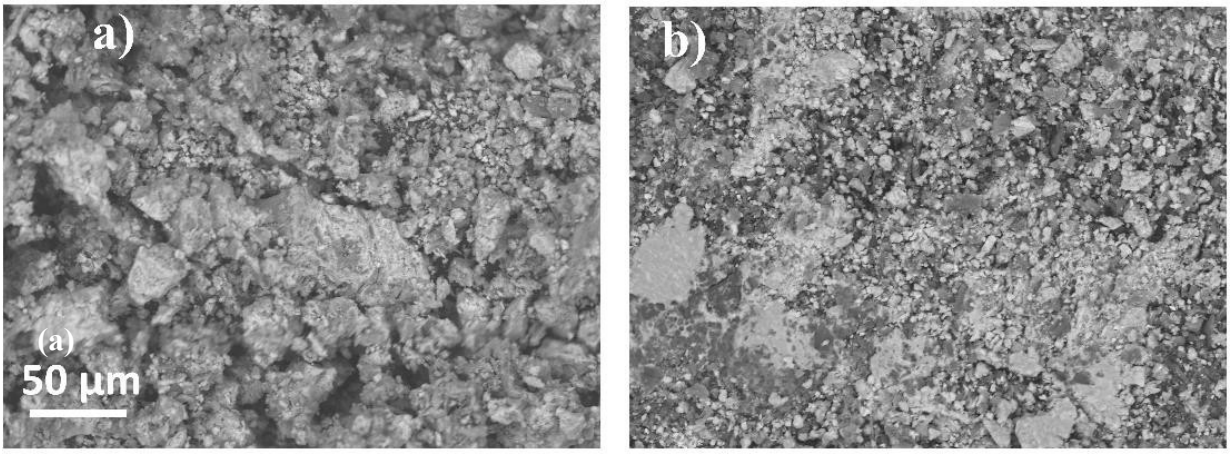

Figure 3: SEM image of samples (a) pure ZnO, (b) 2 % Al-doped ZnO.

The elemental analysis of the samples was carried out and as expected, all of the elements were detected, except for Al, due to its small concentration in the crystal structure.

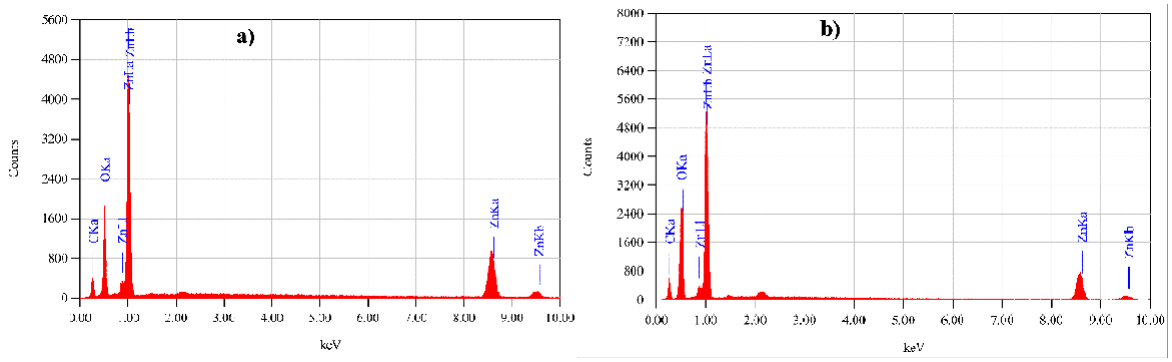

Figure 4: EDS spectra of the un-doped and Al-doped ZnO samples.

The FTIR of undoped and Al-doped Zinc oxide powder samples were analyzed in the wavenumber range from 4000 to 500 cm^{-1} as shown in Figure 5. The band around a wave number of 3428 cm^{-1} is attributed to the stretching of the hydroxyl groups (OH^-), i.e., O-H mode of vibration from adsorbed water molecules (regions I). The sharpness of the peaks is useful for determining the amount of water (H2O) molecule adsorbed on the surface of the samples, which in turn can be used to estimate the amount of the hydroxyl Functional groups adsorbed. The bands at a wavenumber of 1649 and 1450 cm^{-1} are due to the strong asymmetric stretching mode of vibration of C=O (region II and III). The C–O–C bond associated absorption band was

observed at a wavenumber of around 1000 cm^{-1} (region IV). The C–O bonds may be from the precursor material, which is $Zn(CH_3COO)_2.2H_2O$. The characteristic absorption of the Zn- O bond was observed at an absorption band of around 500 cm^{-1}(region V) [20, 25, 27-30].

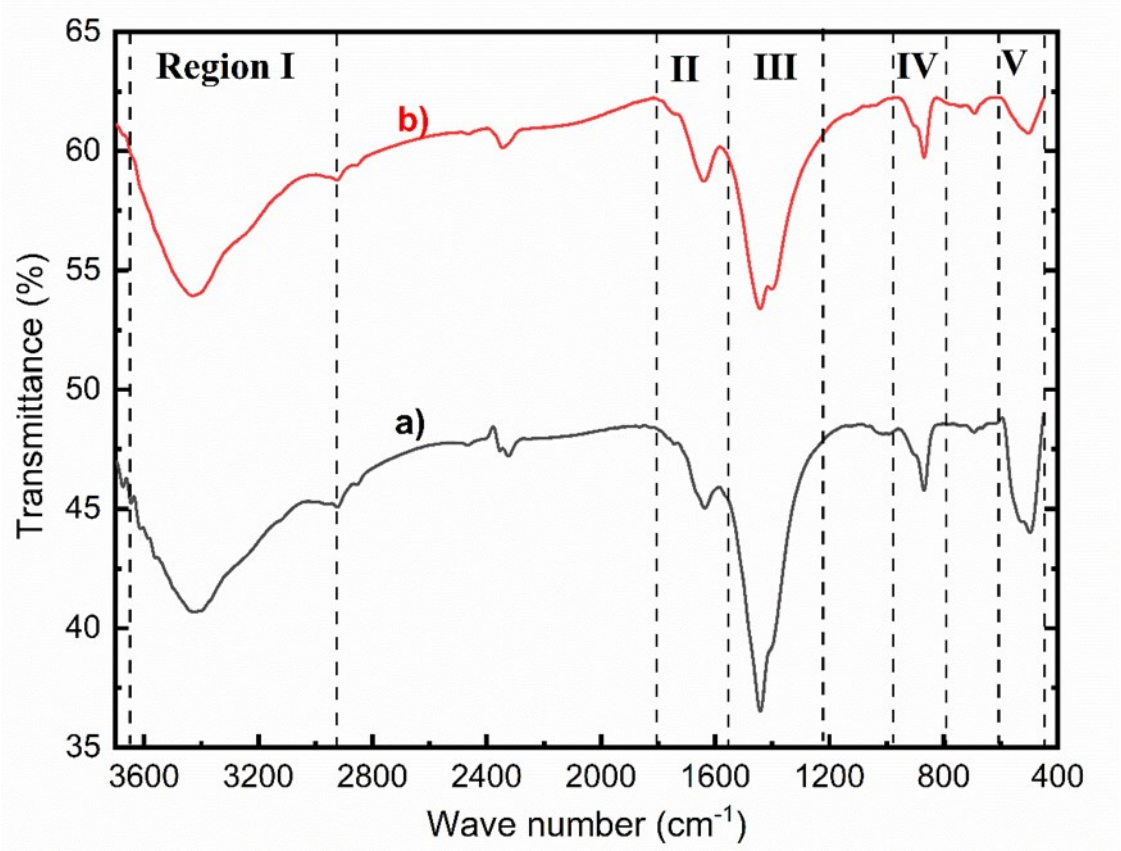

Figure 5: FTIR spectra of undoped (a) and 2% Al-doped ZnO (b).

Figure 6 (a) shows the optical absorption spectra of the different samples, which were measured in the wavelength of 200–900 nm. The optical bandgap energy (Eg) can be calculated from the absorption spectra using Tauc's method, given in equation (3).

$$\alpha hv = \left(hv - E_g\right)^n \quad \textbf{(3)}$$

Here, h is the Plank's constant, v is the frequency of light irradiation, α is the absorption coefficient ($\alpha = 2.303(A/t)$), A is absorbance and t is the thickness of the sample holder or the cuvette. The exponent n depends on the nature of the electronic transition, which is usually ½ for direct bandgap semiconductor materials such as ZnO and its doped states [31]. Rearranging equation (3), the plot of $(\alpha hv)^2$ against (hv) would yield a plot similar to Figure 6 (b) and from the plot of the x-intercept of the tangent line to the linear region of the plot, bandgap energy can be estimated. Therefore, from the intercept, the optical bandgap energies for undoped, 0.5 %, 1%, and 2% Al-doped ZnO, respectively, are about 3.5, 3.0, 2.5, and 2.4 eV, which is in an agreement with the previous works [23, 32-34].

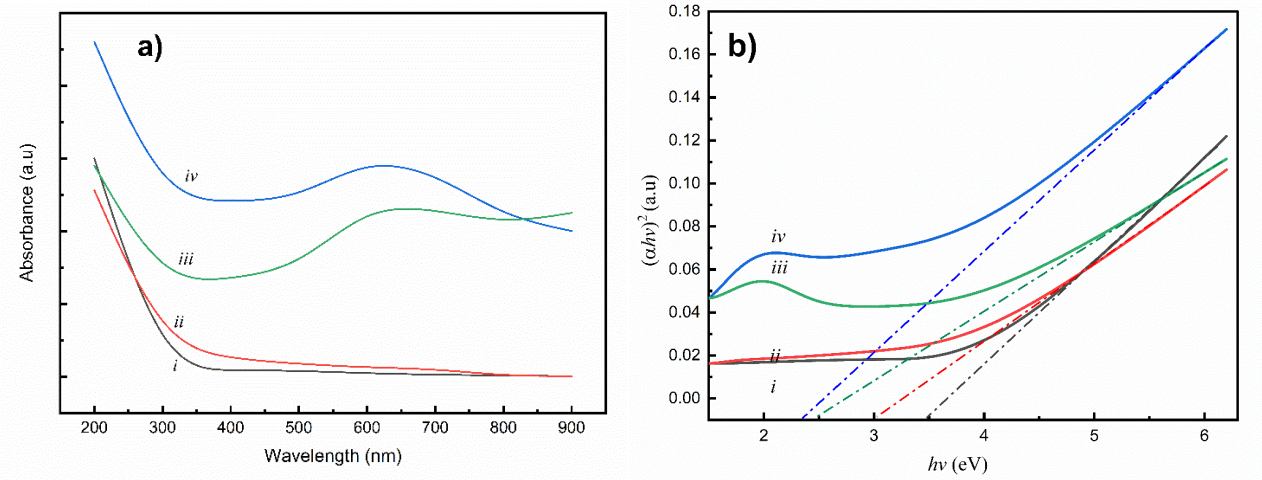

Figure 6: (a) UV absorbance spectra of (i. un-doped ZnO, ii) $Zn_{0.995}Al_{0.005}O$, iii) $Zn_{0.99}Al_{0.01}O$, and iv) $Zn_{0.98}Al_{0.02}O$). (b) Optical band gap energy of (i. un-doped ZnO, ii) $Zn_{0.995}Al_{0.005}O$, iii) $Zn_{0.99}Al_{0.01}O$, and iv) $Zn_{0.98}Al_{0.02}O$).

3.2. Performance evaluation

The photocatalytic performance of the synthesized catalyst was tested for degradation of methylene blue (MB) dye for a wide range of light intensity (3124, 4212, and 5810 lux) and temperature (40, 65, and 80 °C) at different contact time (1, 2, 3 h), The results are presented in **Figure 7 (a-c).**

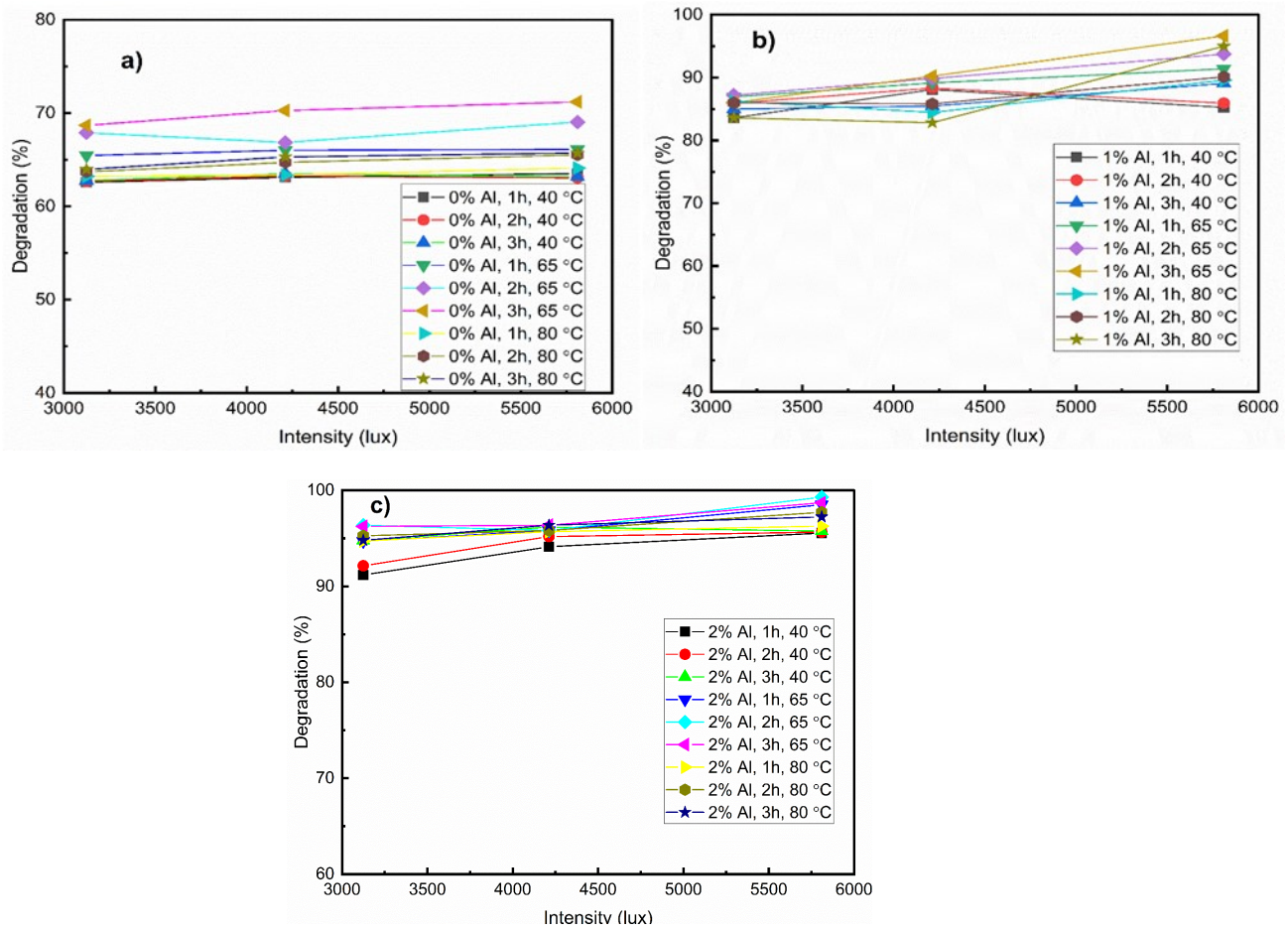

Figure 7: Degradation performance evaluation of (a) un-doped ZnO, (b) $Zn_{0.99}Al_{0.01}O$, and (c) $Zn_{0.98}Al_{0.02}O$ at different light intensity, irradiation times, and degradation temperatures.

As it can be seen in figure 7, it is evident that the degradation performance increased with the increasing percentage of dopant as well as temperature, where the latter showed an optimum performance at around 65 °C. This show that moderate temperature is favorable than lower and high temperature ranges for the photocatalytic degradation process since at higher temperature there is a tendency of recombination of charge carriers that lowers the degradation of the organic molecules while at a lower temperature, the activation energy for degradation could be smaller than the required value [35, 36]. The maximum degradation was obtained at a light intensity of 5810 lux for the sample doped with 2 % Al. Figure 8 shows the effect of degradation temperature on the photo-degradation performance of the catalyst at different irradiation times.

.

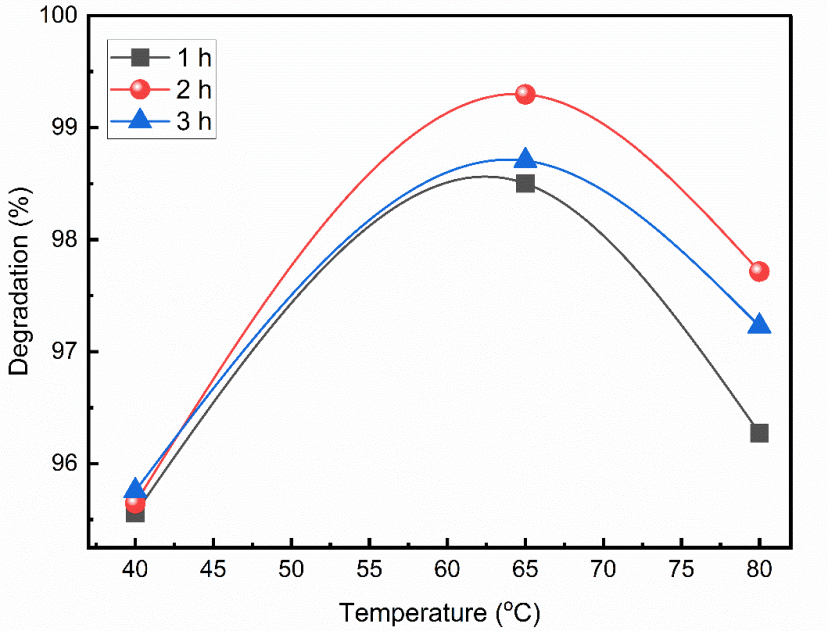

Figure 8: Degradation performance evaluation of $Zn_{0.98}$ $Al_{0.02}O$ at a constant light intensity of 5810 lux and changing the irradiation times and degradation temperatures.

It is evident from the plots of Figure 7 that light intensity has a marginal effect on photocatalytic degradation of methylene blue compared to degradation temperature. As the light intensity increased from 3124 to 5810 lux the degradation percentage increased from about 96 to 99 %, for instance for the sample doped with 2 % Al at a degradation temperature of 65 °C for 2 h degradation time, Figure 7 (c). This is because when photon energy is absorbed on the surface of the samples is increased, the valence band electrons are expected to be excited to the conduction band, while at the same time holes are created in the valence band of the samples. These holes in the valence band can react with water molecules to generate hydroxyl radicals (•OH), while the electrons in the conduction band can react with O_2 molecules to form oxygen radicals ($•O2^-$). These radicals, i.e., both hydroxyl and oxygen radicals, can, in turn, react with the organic dye (the MB) and convert it to H_2O and CO_2 molecules which are non- toxic species [36, 37].

4. Conclusions

Un-doped and Al-doped ZnO were successfully synthesized from their respective precursors via sol-gel route, followed by characterization of the samples. The optical bandgap energies of the samples were evaluated from the UV absorption spectra. Accordingly, the bandgap energies of undoped, 0.5% Al, 1% Al, and 2% Al-doped ZnO were about 3.5, 3.0, 2.5, and 2.4 eV, respectively. Moreover, the dye degradation performance of the samples was investigated by variation of light intensity, degradation times, and temperatures. The 2 % Al-doped ZnO, i.e., $Zn_{0.98}Al_{0.02}O$ showed the highest degradation percentage of above 99 % at a reaction temperature of 65 °C and irradiation time of 2 h. This suggests that using luminescent lamps as a light source and Al-doped ZnO photocatalytic materials, the methylene blue degradation from industrial effluents and aqueous solutions can be realized for remediation of environmental pollutions arising from the non-biodegradable organic dyes.

Acknowledgment

The authors acknowledge Bahir Dar Institute of Technology, Bahir Dar University, for providing financial support for this project.

Reference

1. Jalali, S., et al., *One step integration of plasmonic Ag2CrO4/Ag/AgCl into HKUST-1-MOF as novel visible-light driven photocatalyst for highly efficient degradation of mixture dyes pollutants: Its photocatalytic mechanism and modeling.* Polyhedron, 2019. **166**: p. 217-225.
2. Dai, P., et al., *Silver-loaded ZnO/ZnFe2O4 mesoporous hollow spheres with enhanced photocatalytic activity for 2,4-dichlorophenol degradation under visible light irradiation.* Materials Research Bulletin, 2018. **107**: p. 339-346.
3. David Kuo, H.-W. and I. Xagoraraki, *Contaminants Associated with Drinking Water*, in *International Encyclopedia of Public Health (Second Edition)*, S.R. Quah, Editor. 2017, Academic Press: Oxford. p. 148-158.
4. Zou, L., et al., *Fabrication and dye removal performance of magnetic CuFe2O4@CeO2 nanofibers.* Applied Surface Science, 2015. **332**: p. 674-681.
5. Güy, N. and M. Özacar, *Ag/Ag2CrO4 nanoparticles modified on ZnO nanorods as an efficient plasmonic photocatalyst under visible light.* Journal of Photochemistry and Photobiology A: Chemistry, 2019. **370**: p. 1-11.
6. Mamba, G. and A. Mishra, *Advances in Magnetically Separable Photocatalysts: Smart, Recyclable Materials for Water Pollution Mitigation.* Catalysts, 2016. **6**(6): p. 79.
7. Yang, C.L. and J. McGarrahan, *Electrochemical coagulation for textile effluent decolorization.* J Hazard Mater, 2005. **127**(1-3): p. 40-7.
8. Rodriguez-Narvaez, O.M., et al., *Treatment technologies for emerging contaminants in water: A review.* Chemical Engineering Journal, 2017. **323**: p. 361-380.
9. Adnan, O., et al., *A novel biocoagulant agent from mushroom chitosan as water and wastewater therapy.* Environ Sci Pollut Res Int, 2017. **24**(24): p. 20104-20112.
10. Bellardita, M., et al., *Determination of the crystallinity of TiO2 photocatalysts.* Journal of Photochemistry and Photobiology A: Chemistry, 2018. **367**: p. 312-320.
11. Li, H., et al., *Z-scheme Ag2O/Ag/amorphous TiO2 shells for enhanced plasmonic photoelectrochemical assay of nitrogen dioxide.* Sensors and Actuators B: Chemical, 2019. **289**: p. 138-143.
12. Ma, S., et al., *Photochemical synthesis of ZnO/Ag2O heterostructures with enhanced ultraviolet and visible*

photocatalytic activity. J. Mater. Chem. A, 2014. **2**(20): p. 7272-7280.

13. Wu, H.-Y., et al., *Hierarchical Ag-ZnO Microspheres with Enhanced Photocatalytic Degradation Activities.* Polish Journal of Environmental Studies, 2017. **26**(2): p. 871-880.
14. Guan, Y., et al., *Green one-step synthesis of ZnO/cellulose nanocrystal hybrids with modulated morphologies and superfast absorption of cationic dyes.* Int J Biol Macromol, 2019. **132**: p. 51-62.
15. Zhang, N. and D. Chu, *Fabrication of flower-like hierarchical ZnO nanostructures with enhanced photocatalytic activity.* Surfaces and Interfaces, 2019. **14**: p. 251-255.
16. Praveena, K., et al., *Development of nanocrystalline Mn–Zn ferrites for high frequency transformer applications.* Journal of Magnetism and Magnetic Materials, 2009. **321**(16): p. 2433-2437.
17. Medeiros, S.F., et al., *Stimuli-responsive magnetic particles for biomedical applications.* International Journal of Pharmaceutics, 2011. **403**(1-2): p. 139-161.
18. Niemirowicz, K., et al., *Magnetic nanoparticles as new diagnostic tools in medicine.* Advances in Medical Sciences, 2012. **57**(2): p. 196-207.
19. Abagero, W.B., *Exploring the potentialities of waste plant materials for the production of gold nanoparticles and multi-metallic composite particles and its application in wastewater treatment*. 2017.
20. Alias, S.S. and A.A. Mohamad, *Synthesis of zinc oxide by sol-gel method for photoelectrochemical cells*. 2014: Springer.
21. Chen, X., et al., *Preparation of ZnO photocatalyst for the efficient and rapid photocatalytic degradation of azo dyes.* Nanoscale research letters, 2017. **12**(1): p. 143.
22. Fu, M., et al., *Sol–gel preparation and enhanced photocatalytic performance of Cu-doped ZnO nanoparticles.* Applied Surface Science, 2011. **258**(4): p. 1587-1591.
23. Devi, P.G. and A.S. Velu, *Synthesis, structural and optical properties of pure ZnO and Co doped ZnO nanoparticles prepared by the co-precipitation method.* Journal of Theoretical and Applied Physics, 2016. **10**(3): p. 233-240.
24. Hjiri, M., et al., *Al-doped ZnO for highly sensitive CO gas sensors.* 2014. **196**: p. 413-420.
25. Alias, S., et al., *Effect of pH on ZnO nanoparticle properties synthesized by sol–gel centrifugation.* 2010. **499**(2): p. 231-237.
26. Vanaja, A. and K.S. Rao, *Effect of Co doping on structural and optical properties of zinc oxide nanoparticles synthesized by sol-gel method.* Advances in Nanoparticles, 2016. **5**(01): p. 83.
27. Rehman, I. and W.J.J.o.M.S.M.i.M. Bonfield, *Characterization of hydroxyapatite and carbonated apatite by photo acoustic FTIR spectroscopy.* 1997. **8**(1): p. 1-4.
28. Zhou, G., et al., *Synthesis of amino-functionalized bentonite/CoFe2O4@ MnO2 magnetic recoverable nanoparticles for aqueous Cd2+ removal.* Science of The Total Environment, 2019.
29. Alwan, R.M., et al., *Synthesis of zinc oxide nanoparticles via sol–gel route and their characterization.* 2015. **5**(1): p. 1-6.
30. Bhugul, V. and G. Choudhari, *Synthesis and Studies on Nanocomposites of polypyrrole-Al-doped zinc oxide Nanoparticles.* International Journal of Scientific and Research Publications, 2015. **5**.

31. Janotti, A. and C.G. Van de Walle, *Fundamentals of zinc oxide as a semiconductor.* Reports on Progress in Physics, 2009. **72**(12): p. 126501.
32. Aisah, N., et al. *Synthesis and enhanced photocatalytic activity of Ce-doped Zinc oxide nanorods by hydrothermal method*. in *IOP Conference Series: Materials Science and Engineering*. 2017. IOP Publishing.
33. Aluri, J., et al., *Synthesis and Characterization of ZnO Nanoparticles Using Sol-gel Process.* 2016. **200**(5): p. 45.
34. Ghazai, A.J., E.A. Salman, and Z.A. Jabbar, *Effect of aluminum doping on zinc oxide thin film properties synthesis by spin coating method.* American Scientific Research Journal for Engineering, Technology, and Sciences (ASRJETS), 2016. **26**(3): p. 202-211.
35. Umar, M. and H.A. Aziz, *Photocatalytic degradation of organic pollutants in water*, in *Organic Pollutants- Monitoring, Risk and Treatment*. 2013, IntechOpen.
36. Kumar, S.S., et al., *Synthesis, characterization and optical properties of zinc oxide nanoparticles.* 2013. **3**(1): p. 30.
37. Saravanan, R., F. Gracia, and A. Stephen, *Basic principles, mechanism, and challenges of photocatalysis*, in *Nanocomposites for Visible Light-induced Photocatalysis*. 2017, Springer. p. 19-40.